NANO LETTERS

pubs.acs.org/NanoLett Letter

Complementary Hybrid Semiconducting Superlattices with Multiple Channels and Mutual Stabilization

Jongchan Kim,[#] Chu Thi Thu Huong,[#] Nguyen Van Long, Minho Yoon, Min Jae Kim, Jae Kyeong Jeong, Sungju Choi, Dae Hwan Kim, Chi Ho Lee, Sang Uck Lee, and Myung Mo Sung*

Cite This: *Nano Lett.* 2020, 20, 4864−4871 Read Online

ACCESS | Metrics & More | Article Recommendations | Supporting Information

ABSTRACT: An organic−inorganic hybrid superlattice with near perfect synergistic integration of organic and inorganic constituents was developed to produce properties vastly superior to those of either moiety alone. The complementary hybrid superlattice is composed of multiple quantum wells of 4-mercaptophenol organic monolayers and amorphous ZnO nanolayers. Within the superlattice, multichannel formation was demonstrated at the organic−inorganic interfaces to produce an excellent-performance field effect transistor exhibiting outstanding field-effect mobility with band-like transport and steep subthreshold swing. Furthermore, mutual stabilizations between organic monolayers and ZnO effectively reduced the performance degradation notorious in exclusively organic and ZnO transistors.

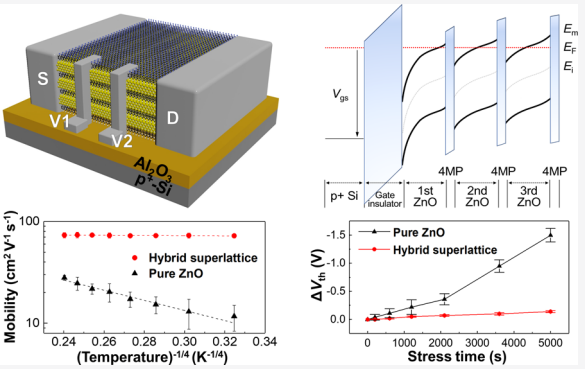

KEYWORDS: *hybrid superlattices, complementary, multiple channels, mutual stabilization*

INTRODUCTION

Hybrid organic−inorganic materials have been exploited as a very unique and promising class of artificial materials combining the distinct properties of the individual organic and inorganic components.[1−5] They are widely used to improve optical[6] and magnetic properties,[7] luminescence,[8] electrical,[9] thermal,[10] and ionic conductivity,[11] and chemical reactivity.[12] Therefore, hybrid materials have been exploited for numerous applications such as organic light-emitting diodes (OLEDs),[13] solar cells,[14] energy storage,[15] functional coatings,[16] catalysis,[17] optics,[6] electronics,[18] and sensors.[19] However, hybrid materials suffer from structural irregularity and incompatible nature between organic and inorganic constituents.[1−3] One promising solution is development of layered organic−inorganic superlattices with a periodic structure. Within the superlattice structure, a synergic combination of organic and inorganic constituents produces new, useful functions or properties that neither moiety demonstrates alone. Theoretically, a complementary hybrid superlattice with perfect synergy of the properties inherent to the different classes of materials can be developed with a regular structure.

Thin-film transistors (TFTs) are the most popular design of pixel switches in cutting-edge displays such as active-matrix and micro light-emitting diodes and virtual and augmented reality (VR and AR, respectively) devices.[20−22] Interestingly, as TFTs have enhanced area/energy efficiency and power, high-performance TFT-based integrated circuits (ICs) are recognized as a potential replacement for silicon (Si) complementary metal-oxide semiconductors (CMOS).[23] Thin-film ICs are becoming the ideal technology for diverse types of wearable Internet of things (IoT) devices that allow communication between humans and/or smart devices because thin-film ICs can be lightweight, flexible, scalable, low-cost and biocompatible.[23] Currently, low-temperature polycrystalline silicon (LTPS) and oxide semiconductors are the most mature technologies for TFT channel layers,[20,24] while diverse candidates, such as amorphous Si (a-Si),[25] organic,[26] superlattice,[27] and two-dimensional (2D) semiconductors,[28] have been proposed. LTPS has been a prominent option owing to its high field-effect mobility (μ > 100 $cm^2\ V^{-1}\ s^{-1}$), but it still suffers from lack of uniformity due to grain boundaries in the polycrystalline structure and high-cost manufacturing processes such as excimer laser crystallization (ELC).[20,24] Amorphous oxide semiconductors are more attractive to commercial electronics than is LTPS because they have far more reproducible large-area fabrication and are less expensive.[24] However, there are critical issues of these semiconductors that must be overcome for practical

Received: February 26, 2020
Revised: June 15, 2020
Published: June 18, 2020

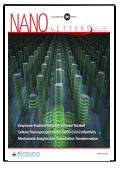

https://dx.doi.org/10.1021/acs.nanolett.0c00859
Nano Lett. 2020, 20, 4864−4871

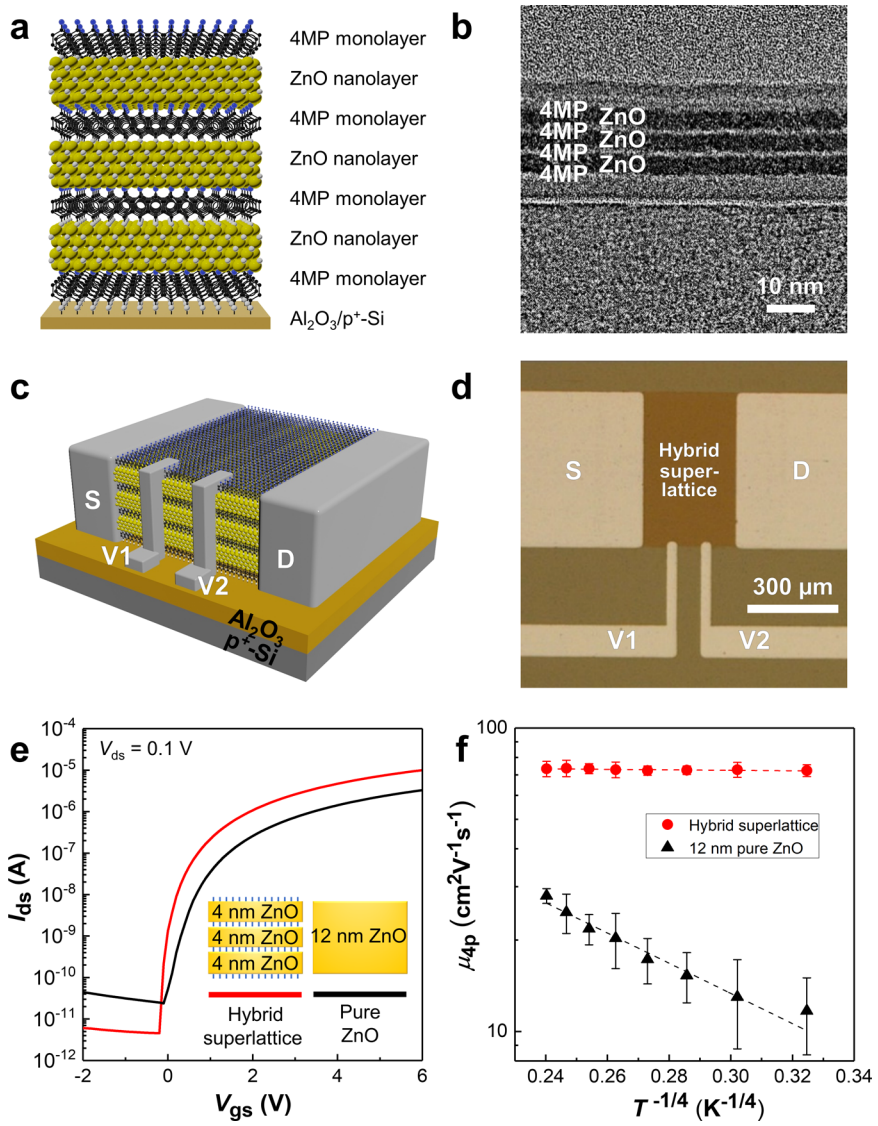

Figure 1. Complementary 4MP/ZnO hybrid superlattices. (a) Model structure and (b) cross-sectional transmission electron microscopy (TEM) image of the triple-quantum-well 4MP/ZnO superlattice. (c) Schematic image and (d) optical micrograph of the bottom-gate top-contact FET with four-probe electrodes based on the triple-quantum-well superlattice. (e) Typical transfer (I_{ds}–V_{gs}) characteristics of FETs with the triple-quantum-well superlattice and the 12 nm pure ZnO thin film as channel materials (Inset). (f) Temperature-variable intrinsic mobilities (μ_{4p}) plotted against $T^{-1/4}$ for the two FETs with hybrid superlattice or pure ZnO. Total ZnO thickness for all samples was maintained at 12 nm.

application, such as inferior field-effect mobility (μ < 40 cm^2 V^{-1} s^{-1})[23,29] and poor bias stability.[30,31] Regarding the poor bias stability, minimization of degradation under bias stress has been attempted through encapsulation[16] or annealing,[31] but there is no strategy for enhancing their intrinsic stability. Recently, various heterostructures have been offered to effectively engineer field-effect mobility with modulation doping to form a two-dimensional electron gas (2DEG).[32−36] Nevertheless, the mobility is still far from that needed for practical applications for VR/AR displays beyond human retina resolution or high-performance thin-film IoT ICs, and doping can increase power dissipation due to increased source-drain current in the OFF-state (I_{OFF}).[23]

Herein, we report a new complementary hybrid semiconducting superlattice composed of alternating 4-mercaptophenol (4MP) organic monolayers and ZnO nanolayers. Within the hybrid superlattice, complementary hybridization of 4MP monolayers and ZnO nanolayers produces extraordinary enhancement of both electrical performance and stability compared to those of each moiety alone. The improvement in electrical characteristics mainly originated in multichannel formation in the superlattice with quantum confinement of ZnO nanolayers. Accordingly, the transistors with a hybrid superlattice as an active channel exhibited higher field-effect mobility and steeper subthreshold swing compared with the pure ZnO transistors. In the hybrid superlattice, only a 4MP monolayer was incorporated between ZnO nanolayers as an organic constituent to minimize deterioration of the semiconducting properties, a frequent issue in hybrid materials. Furthermore, owing to mutual stabilization between 4MP and ZnO, performance degradation notorious in organic and ZnO transistors was successfully avoided. Chemical bonds cross-linking the components stabilize the organic monolayers against easy decomposition and prevent formation of detrimental defects at the surfaces of ZnO nanolayers. In addition, the organic monolayers in the superlattices provide

https://dx.doi.org/10.1021/acs.nanolett.0c00859
Nano Lett. 2020, 20, 4864−4871

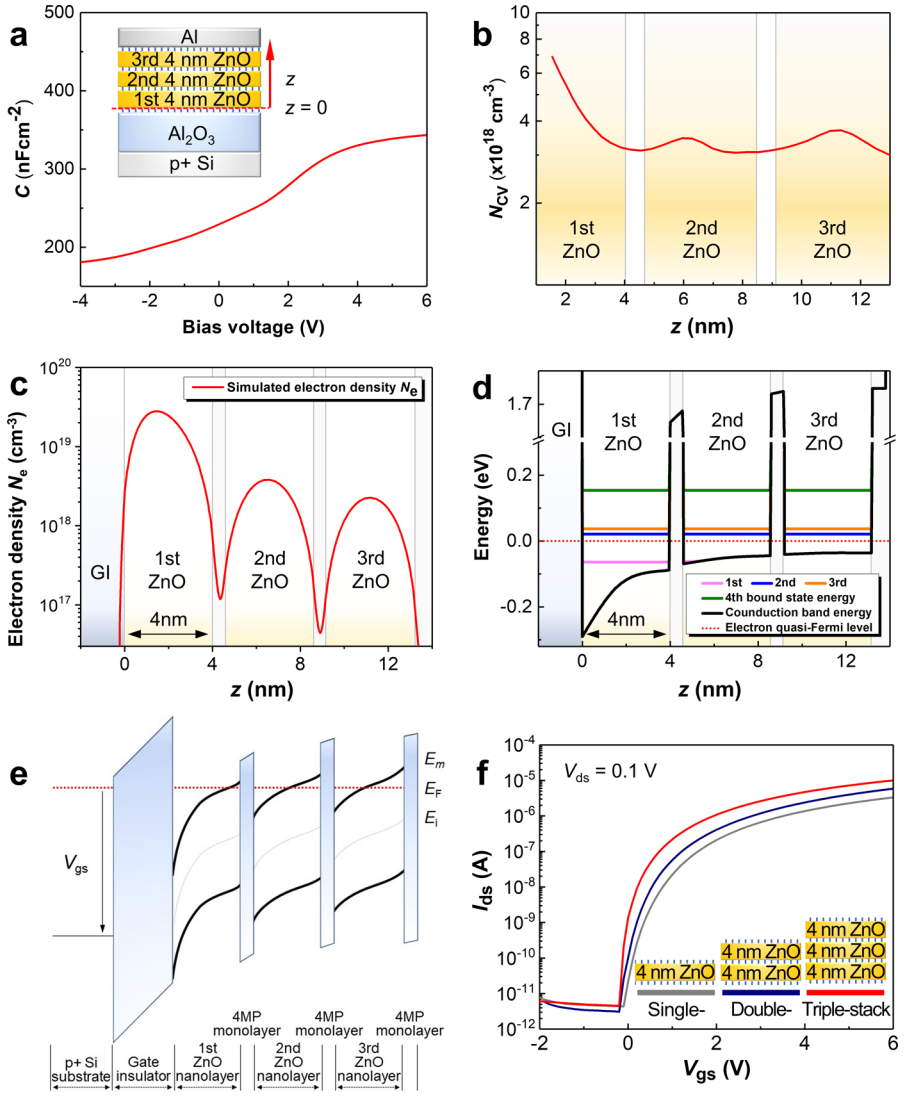

Figure 2. Multichannel formation in the hybrid superlattices. (a) Capacitance−voltage ($C-V$) characteristics of the triple-quantum-well superlattice capacitor. The inset shows a schematic structure of the corresponding metal−insulator−semiconductor (MIS) capacitor. (b) Depth profile of the carrier concentration extracted from (a). (c) Simulated free electron density distribution (N_e) along the vertical direction at the gate-source voltage (V_{gs}) of 6 V and (d) corresponding energy band diagram of the hybrid superlattice transistor. (e) Schematic band diagram of the triple-quantum-well superlattice FET in the ON-state. (f) Transfer characteristics for single-, double-, and triple-quantum-well FETs. The inset shows schematic representation of the superlattice active channels.

good mechanical flexibility to the inorganic framework, allowing the superlattice transistor on plastic substrates to resist drastic bending stress.

RESULTS AND DISCUSSION

Complementary organic−inorganic semiconducting superlattices were fabricated using molecular layer deposition (MLD) and atomic layer deposition (ALD) to form 4-mercaptophenol (4MP) organic monolayers and ZnO inorganic nanolayers, respectively (Figure 1a). See the Supporting Information for the detailed fabrication. Cross-sectional transmission electron microscopy (TEM) was used to identify the hybrid superlattice with triple quantum wells (Figure 1b). The 4MP organic monolayers were identified in the image by color contrast. The TEM image confirmed that the individual 4MP monolayers and ZnO nanolayers constituted the superlattice with good interfaces. Additionally, the measured thickness of the 4MP monolayer was approximately 7 Å, indicating that the organic chain was only tilted 17° from the surface normal, which corresponds to the theoretically predicted value of 14° from the optimized 4MP/ZnO superlattice structure in Figure S1 (Supporting Information). The thickness of the ZnO nanolayers was controlled by adjusting the number of ALD cycles with a growth rate of 1.43 Å per cycle. The ZnO thickness was 4 nm, the same as expected for 28 ALD cycles. The ZnO nanolayers in the superlattice were amorphous, which was confirmed by high-resolution TEM and X-ray diffraction (XRD) (Figure S2, Supporting Information). Atomic force microscopy (AFM) images of the hybrid superlattices showed very smooth and uniform surfaces, and the root-mean-square (RMS) roughness of the surfaces was as small as 0.33 nm (Figure S3, Supporting Information). The RMS roughness of the initial cleaned silicon substrate was approximately 0.22 nm.

Bottom-gate top-contact field effect transistors (FETs) adopting the superlattice as an active channel (Figure 1c)

https://dx.doi.org/10.1021/acs.nanolett.0c00859
Nano Lett. 2020, 20, 4864−4871

were fabricated to evaluate the electrical characteristics of the resultant organic−inorganic hybrid superlattice containing three 4 nm thick ZnO nanolayers sandwiched between 4MP organic monolayers. See the Supporting Information for the detailed procedure and capacitance measurement (Figure S4). For extracting the intrinsic electrical properties from the FETs, a four-point probe configuration (Figure 1d) was used to eliminate any contact effect (Figure S5, Supporting Information).[37] Figure 1e displays the typical $I_{ds}-V_{gs}$ transfer characteristics of the hybrid superlattice (red) and pure ZnO (black) transistors, where I_{ds}, V_{ds}, and V_{gs} are the drain-source current and drain- and gate-source voltage, respectively. The insets in Figure 1e show the schematics corresponding to the two channel structures. A typical pure-ZnO FET exhibits conventional n-type transfer characteristics: the intrinsic electron field-effect mobility (μ_{4p}) is estimated to be 28 cm^2 V^{-1} s^{-1} along with an on/off current ratio of 10^5 and a subthreshold swing (SS) deduced as 225 mV $decade^{-1}$ from the linear fitting of the transfer curve (Figure S5, Supporting Information). These are comparable to those previously reported for high-performance ZnO FETs.[38] However, the typical hybrid superlattice FET shows notably enhanced electrical performance: the intrinsic mobility (μ_{4p}) reached 73 cm^2 V^{-1} s^{-1} with a high on/off current ratio of 10^6 and an excellent SS as steep as 110 mV $decade^{-1}$. Table S1 in the Supporting Information summarizes theelectrical characteristics of the typical superlattice FET versus the pure ZnO transistor.

To evaluate the charge transport mechanism, we performed temperature-variable measurements from 300 to 90 K for FETs with the hybrid superlattice or 12 nm pure ZnO. Figure 1f displays the temperature-dependent μ_{4p} of the superlattice (red) and pure ZnO (black) FETs. For the pure ZnO FET, the intrinsic mobility consistently drops over the entire temperature range (300−90 K) as the temperature decreased. Logarithmic mobility values as a function of temperature follow the relationship $\ln(\mu_{4p}) \sim -T^{-1/4}$. This result is clearly explained by a thermally activated behavior with an activation energy of 15 meV (Figure S5, Supporting Information), which is consistent with earlier reports for many amorphous oxide semiconductors and is related to hopping conduction.[39,40] However, the hybrid superlattice FETs exhibited no temperature dependence on the intrinsic mobility value of 73 cm^2 V^{-1} s^{-1} over 300−90 K, which can be explained by a band-like transport model.[32,35,41] In contrast to the pure ZnO FETs displaying the hopping conduction, the observation of band-like transport in the hybrid superlattice FETs suggests that the inherent drawbacks of amorphous ZnO can be overcome by the complementary hybrid semiconducting superlattices to produce high-performance FETs.[32−35]

Analysis of the unique charge carrier distribution in the triple-quantum-well superlattice was performed for in-depth understanding of electrical performance enhancement in the superlattice FETs. Capacitance−voltage ($C-V$) depth profiling is a useful technique to allow depth analysis of the carrier concentration in semiconducting thin films.[32,34,36] For this analysis, metal−insulator−semiconductor (MIS) capacitors with the superlattice were fabricated as shown in the inset of Figure 2a. The obtained $C-V$ characteristics from the superlattice capacitor (Figure 2a) show an increase in total capacitance per unit area (C) with bias voltage (V), and depletion (V < 1.5 V) and accumulation (V > 4.0 V) regions are separated. Using the depth profiling method (Figure S6, Supporting Information), the $C-V$ characteristics were transformed into spatial distribution of the carrier concentration across the channel depth (z) by setting the origin (z = 0) at the bottom of the first ZnO nanolayer.[32,34,36] Significantly, the depth profile of the carrier concentration (Figure 2b) shows two additional peaks at z = 6.2 and 11.2 nm, both evidently corresponding to the confined charge carriers in the second and third ZnO nanolayers of the superlattice, respectively. In comparison, MIS capacitors with 12 nm pure ZnO thin films were fabricated to show no additional peak in the depth profile of carrier concentration (Figure S6, Supporting Information). Therefore, carrier distribution analysis clarified formation of multiple channels in an organic−inorganic hybrid superlattice, which could be related to improvement in electrical performance.

Multichannel formation in the hybrid superlattice FET was theoretically expected by technological computer-aided design (TCAD) simulations carried out using Silvaco ATLAS-2D self-consistent solution of the Schrödinger−Poisson model. Simulation parameters are listed in Table S2 and S3 (Supporting Information). The free electron density distributions (N_e) and energy band diagrams for the 12 nm pure ZnO or hybrid superlattice channels along the vertical direction from the dielectric/channel interface toward the back-channel surface were calculated as shown in Figure 2c,d and Figure S7 (Supporting Information). As expected, the maximum N_e value was near the interfacial channel/dielectric region for the 12 nm pure ZnO FET (Figure S7, Supporting Information) and decreased rapidly toward the back-channel surface. As shown in Figure 2c, the triple-quantum-well superlattice FET exhibited three distinct local maxima near the centroid of each ZnO nanolayer, which is consistent with $C-V$ analysis. The wave function of conduction electrons can be confined effectively in each potential well of the ZnO nanolayer due to the potential barrier of the 4MP monolayer, which generates quasi 2-dimensional electron gas (2DEG) within the hybrid superlattice. The existence of quasi 2DEG with these parallel multichannels and minimized scattering of quasi 2DEG at the heterointerface due to local N_e minima allow synergic enhancement of the carrier mobility and SS of the resulting field-effect transistors. Furthermore, all TCAD-simulated transfer characteristics accurately reproduced the measured $I-V$ data with excellent fit (Figure S8, Supporting Information), indicating that our physical model is valid and adequate to predict device performance.

On the basis of experimental and theoretical depth analyses of charge carrier distribution for triple-quantum-well superlattice devices, we propose a schematic band diagram in Figure 2e under V_{gs} beyond the threshold voltage (V_{th}). Here, formation of multiple channels was established by additive band bendings at the 4MP/ZnO interfaces, where induced surface charges are generated in response to an electric field due to discontinuity in polarizability between ZnO and 4MP. As shown in Figure 1e,f, where the hybrid superlattice FETs showed higher μ_{4p} value with temperature independence in contrast to pure ZnO FET, multichannel formation in the superlattice mainly demonstrates critical enhancement in FET performance. Figure 2e shows that the band bendings at the 4MP/ZnO interfaces effectively reduced the gap between the Fermi level (E_F) and mobility edge (E_m) to increase the free electron density throughout the superlattice channels, which eventually improved the mobility (μ_{4p}) with band-like transport.[41] Additionally, multichannel formation produces

https://dx.doi.org/10.1021/acs.nanolett.0c00859
Nano Lett. 2020, 20, 4864−4871

steep SS for the superlattice FET because trap states in each ZnO nanolayer are simultaneously filled.[34]

Furthermore, the number of stacked quantum wells was carefully examined to understand the multichannel effect on the superlattice FETs associating quantum confinement of the ZnO nanolayer. First, the single-quantum-well FET exhibits similar μ_{4p} and steeper SS compared to the 12 nm pure ZnO FET (Figure 2f). Notably, the μ_{4p} plot versus $T^{-1/4}$ for the single-quantum-well FET exhibited no temperature dependence over the temperature range of 300−90 K (Figure S9, Supporting Information), implying band-like transport. This result suggests the existence of a quasi 2DEG in the ZnO nanolayer due to the confined charge carriers near the center of the quantum well,[42,43] as expected by TCAD simulation. Given the quasi 2DEG in the ZnO nanolayer, SS for the single-quantum-well FET was additionally suppressed.[43] Additionally, enhancement of FET characteristics was investigated by increasing the number of stacked quantum wells three times. Figure 2f and Table 1 show gradual enhancement of FET performance with increase in number of stacked quantum wells, such as increasing μ_{4p} and reducing SS, ensuring formation of multiple channels in hybrid superlattice FETs. These results suggest that multichannel formation enables the hybrid superlattice FETs to have higher μ_{4p} with band-like transport and steeper SS compared to pure ZnO, by inducing more charge carriers occupying extended states at the 4MP/ZnO interfaces. Therefore, the results pave the way for engineering FET performance by simply constructing a multiple quantum well structure to modify the distribution of accumulation layers therein.

Table 1. FET Characteristics for Single-, Double-, and Triple-Quantum-Well FETs

	single quantum well	double quantum well	triple quantum well
μ_{4p} ($cm^2\ V^{-1}\ s^{-1}$)	30	50	73
I_{ON}/I_{OFF}	7.2×10^5	1.8×10^6	2.2×10^6
I_{OFF} (A)	4.6×10^{-12}	3.2×10^{-12}	4.5×10^{-12}
SS (mV $decade^{-1}$)	165	140	110

We applied the complementary hybrid superlattice in large-scale flexible electronics. A wafer-scale FET array containing 284 transistors was fabricated on a 4 in. polyimide (PI) substrate (Figure 3a). Please refer to Supporting Information for detail in fabrication. Statistical distributions of the two-probe mobilities (μ_{2p}) and on/off current ratios (I_{ON}/I_{OFF}) are demonstrated as histograms in Figure 3b,c, respectively. Quantitatively, the μ_{2p} data set highly converged to the average value of 52.7 ($\pm$1.13) $cm^2\ V^{-1}\ s^{-1}$, and the average I_{ON}/I_{OFF} was also good, with a value of 2.8 ($\pm$0.9) $\times\ 10^6$. Overall, the resultant device-to-device uniformity and reproducibility were outstanding compared to oxide semiconductor FETs,[36,44] confirming the feasibility of our hybrid superlattice FETs for large-area applications.

The 4MP/ZnO superlattice with triple-quantum-well is a promising semiconductor channel because of its high μ_{2p}, steep SS, low I_{OFF}, superior uniformity, and low-temperature processability. Furthermore, highly improved bias-illumination stability of the superlattice FET can unravel an important issue for developing practical products. To elaborate on electrical stability, negative bias illumination stress (NBIS) tests were carried out. Parts d and e of Figure 3 present the time-dependent transfer characteristics under NBIS for the hybrid superlattice and pure ZnO FETs, respectively. As summarized in Figure 3f, the superlattice FET revealed excellent stabilities over the stress time, with nonsignificant variations of V_{th} (ΔV_{th}) and SS (ΔSS), unlike the pure ZnO FETs that suffered from unstable electrical behavior.[45] In addition, various gate-bias stability tests including positive bias stress (PBS), negative bias stress (NBS), and positive bias illumination stress (PBIS) also confirmed the nearly unchanged performance of the hybrid superlattice FET (Figure S10, Supporting Information). These results indicate that 4MP/ZnO hybrid superlattices surpass bias and illumination stability of oxide semiconductors.[46,47] Note that the hybrid superlattices were also thermally stable in the air up to 300 °C.

The high stability of the 4MP/ZnO hybrid superlattice can be explained by another complementary hybridization between 4MP organic monolayers and ZnO nanolayers, called mutual stabilization. The 4MP monolayer itself has preeminent stability compared with that for typical MLD-grown organic monolayers, such as alucone and zincone, due to the air-stable Zn−S bond and $\pi-\pi$ stacking of aromatic rings.[48] Nevertheless, as an inherent drawback of free-standing organic molecules, a lack of chemical bonding between the tail groups in a free-standing 4MP monolayer generates disorder and physicochemical instability.[49] In our hybrid superlattice, the head and tail groups of the 4MP molecules were covalently bonded to the adjacent ZnO cross-linkers to stabilize themselves (Figure 1a).[49] Furthermore, we executed density functional theory (DFT) calculations to gain further insights into the effect of 4MP molecules to functionalize ZnO surface by evaluating oxygen defect formation energy (E^f_{VO}). Using the theoretically designed hybrid 4MP/ZnO structure (Figure S1, Supporting Information), E^f_{VO} were calculated by considering all possible defect sites (Figure 3g and Figure S11, Supporting Information) on the (001) surface of the pure ZnO and hybrid 4MP/ZnO structures. The remarkably higher E^f_{VO} value of 3.995 eV for the hybrid 4MP/ZnO was obtained versus 0.277 eV of pure ZnO (Table S4, Supporting Information), which implies that the hybrid superlattice is extremely resistant to oxygen defect formation. To elaborate on oxygen defect formation, we deeply analyzed the electronic states using the projected density of states (PDOS) on oxygen because the frontier states near the Fermi level are mainly involved in defect formation reaction. As expected, the PDOS analysis in Figure 3h,i and Figure S11 (Supporting Information) shows that the surface oxygens of both pure ZnO and hybrid 4MP/ZnO dominantly contribute to frontier states compared to core oxygens. Therefore, oxygen defects are liable to occur on the surface of pure ZnO and hybrid 4MP/ZnO. However, hybrid 4MP/ZnO has an interesting PDOS behavior depending on position of surface oxygens, where the PDOS of oxygen close to 4MP shifts down from the Fermi level. Consequently, more energy is needed to form defects of oxygen close to 4MP. Oxygen vacancy states were experimentally measured using X-ray photoelectron spectroscopy (XPS) analysis in both the pure ZnO and the hybrid superlattice thin films. The results show that the vacancy concentration for the hybrid superlattice was much smaller than that for pure ZnO (Figure S12, Supporting Information). Consequently, the characteristic electronic features of the 4MP/ZnO hybrid semiconducting superlattice can efficiently suppress oxygen defect formation on the surface, minimizing the performance degradation common in ZnO FETs.

https://dx.doi.org/10.1021/acs.nanolett.0c00859
Nano Lett. 2020, 20, 4864−4871

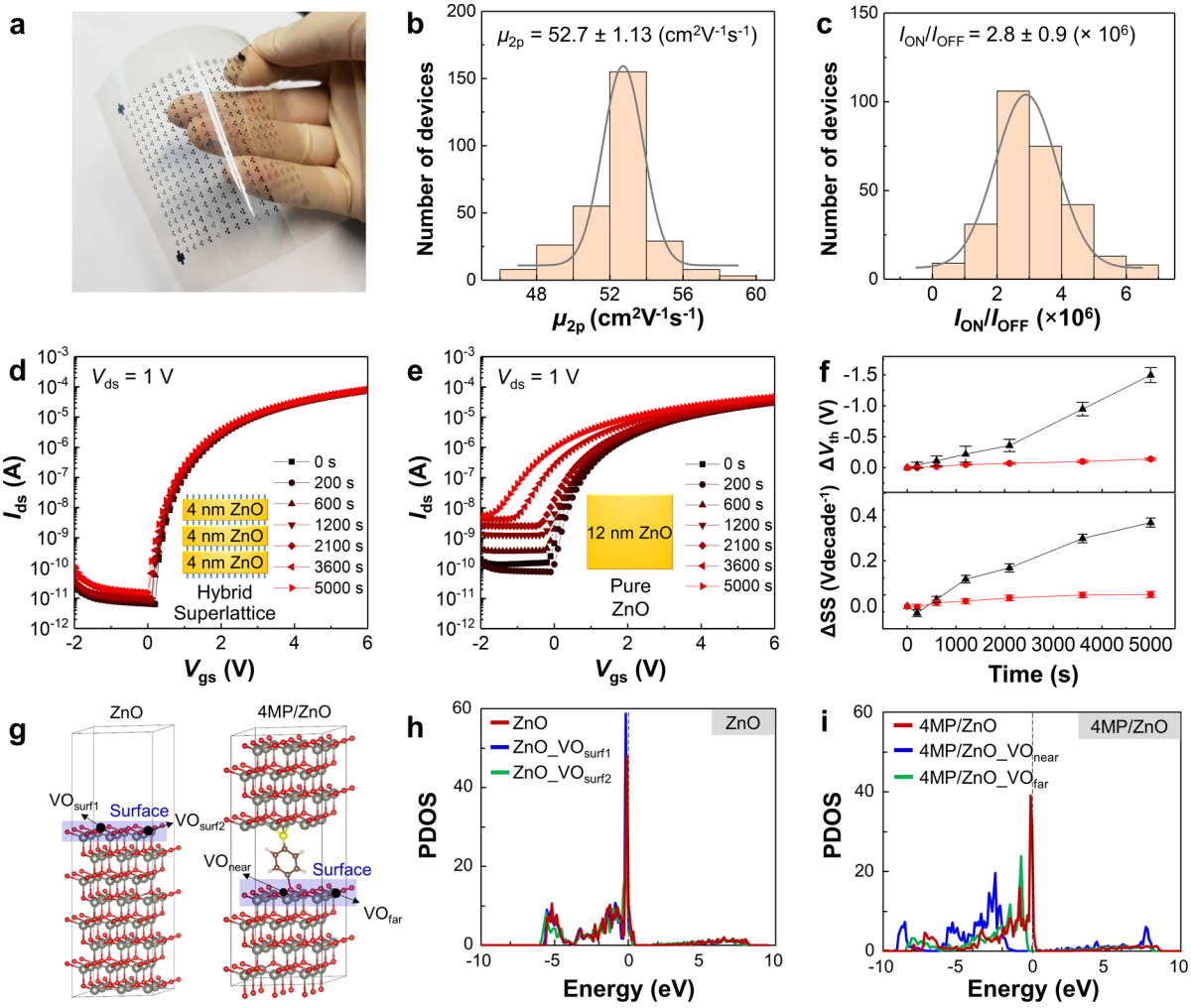

Figure 3. Large-area complementary hybrid superlattice FETs. (a) Photograph of an array containing 284 superlattice FETs on a 4 in. polyimide (PI) substrate. (b) Two-probe mobility (μ_{2p}) and (c) on/off current ratio (I_{ON}/I_{OFF}) distributions for 284 FETs with the triple-quantum-well superlattice on PI substrate. (d, e) Transfer characteristics under negative bias illumination stress (NBIS) as a function of stress time for the (d) superlattice and (e) 12 nm pure ZnO FETs. (f) Threshold voltage shift (ΔV_{th}) and subthreshold swing shift (ΔSS) as a function of stress time for the superlattice and pure ZnO FETs. (g) Atomic model structures for the (001) surface of pure ZnO (left) and hybrid 4MP/ZnO (right). (h, i) Projected density of states (PDOS) on oxygens for (h) the pure ZnO surface and (i) hybrid 4MP/ZnO surface.

For flexible electronics that require the ability to be folded without loss of performance, electrical properties of hybrid superlattice FETs on PI were investigated after repetitive bending up to 10000 cycles with a 1 mm bending radius. The variation of transfer characteristics as a function of bending cycles (Figure S13, Supporting Information) exhibits excellent mechanical flexibility to provide great endurance to external strain due to the ultrathin ZnO nanolayers sandwiched between the 4MP organic monolayers. Additionally, Figure S14 (Supporting Information) shows the transmittance spectra of the triple-quantum-well superlattice on a quartz wafer, which clearly illustrates high transparency that exceeded 90% in the visible light range. The 4MP/ZnO hybrid superlattice FETs reveal potential use in flexible and invisible electronics due to its endurance of strenuous bending and transparency over the visible light range.

CONCLUSIONS

A new 4MP/ZnO hybrid semiconducting superlattice with extraordinary enhancement of both electrical performance and stability was developed through complementary hybridizations of the two constituents. The significant improvements mainly originated in multichannel formations in the hybrid superlattice and mutual stabilizations between 4MP and ZnO nanolayers. As a result, hybrid superlattice FETs exhibited remarkable electrical properties, such as a high mobility μ_{4p} of 73 $cm^2\ V^{-1}\ s^{-1}$, an excellent subthreshold swing as steep as 110 mV $decade^{-1}$, and exceptional stabilities. This study suggests a new design rule for engineering FET performance by developing organic−inorganic hybrid materials employing the regular superlattice structure with optimized complementary integration of the two constituents.

ASSOCIATED CONTENT

Supporting Information

The Supporting Information is available free of charge at https://pubs.acs.org/doi/10.1021/acs.nanolett.0c00859.

Methods, model structures for DFT calculation, XRD and AFM data, geometric capacitance of Al_2O_3 dielectric, intrinsic mobility extraction, $C-V$ depth profiling equation and the result from pure ZnO capacitor, TCAD result of pure ZnO transistor,

https://dx.doi.org/10.1021/acs.nanolett.0c00859
Nano Lett. 2020, 20, 4864−4871

simulated transfer curves, characterization of single-quantum-well FET for 300−90 K, stability test under various stresses, detailed PDOS analysis, oxygen vacancy analysis, bending test, transmittance spectra, electrical characteristics compared with pure ZnO transistor, TCAD parameters, sequential defect formation energies (PDF)

AUTHOR INFORMATION

Corresponding Author

Myung Mo Sung − *Department of Chemistry, Hanyang University, Seoul 04763, Republic of Korea;* orcid.org/0000-0002-2291-5274; Email: smm@hanyang.ac.kr

Authors

Jongchan Kim − *Department of Chemistry, Hanyang University, Seoul 04763, Republic of Korea*

Chu Thi Thu Huong − *Department of Chemistry, Hanyang University, Seoul 04763, Republic of Korea*

Nguyen Van Long − *Department of Chemistry, Hanyang University, Seoul 04763, Republic of Korea;* orcid.org/0000-0002-5665-1019

Minho Yoon − *Department of Chemistry, Hanyang University, Seoul 04763, Republic of Korea;* orcid.org/0000-0003-3096-6116

Min Jae Kim − *Department of Electronic Engineering, Hanyang University, Seoul 04763, Republic of Korea*

Jae Kyeong Jeong − *Department of Electronic Engineering, Hanyang University, Seoul 04763, Republic of Korea;* orcid.org/0000-0003-3857-1039

Sungju Choi − *C-ICT Research Center (ERC), School of Electrical Engineering, Kookmin University, Seoul 02707, Republic of Korea*

Dae Hwan Kim − *C-ICT Research Center (ERC), School of Electrical Engineering, Kookmin University, Seoul 02707, Republic of Korea;* orcid.org/0000-0003-2567-4012

Chi Ho Lee − *Department of Applied Chemistry, Hanyang University, Ansan 15588, Republic of Korea;* orcid.org/0000-0002-0127-0059

Sang Uck Lee − *Department of Applied Chemistry, Hanyang University, Ansan 15588, Republic of Korea;* orcid.org/0000-0001-9596-2349

Complete contact information is available at: https://pubs.acs.org/10.1021/acs.nanolett.0c00859

Author Contributions

[#]J.K. and C.T.T.H. contributed equally to this work.

Funding

This work was supported by Samsung Research Funding Center of Samsung Electronics under Project Number SRFC-TA1703-12.

Notes

The authors declare no competing financial interest.

ACKNOWLEDGMENTS

The authors gratefully acknowledge Prof. Kyeongjae Cho for the insightful discussion in density functional theory (DFT) calculations.

REFERENCES

(1) Mitzi, D. B.; Chondroudis, K.; Kagan, C. R. Organic − Inorganic Electronics. *IBM J. Res. Dev.* **2001**, *45*, 29−45.

(2) Saveleva, M. S.; Eftekhari, K.; Abalymov, A.; Douglas, T. E. L.; Volodkin, D.; Parakhonskiy, B. V.; Skirtach, A. G. Hierarchy of Hybrid Materials-the Place of Inorganics-in-Organics in It, Their Composition and Applications. *Front. Chem.* **2019**, *7*, 179.

(3) Mir, S. H.; Nagahara, L. A.; Thundat, T.; Mokarian-Tabari, P.; Furukawa, H.; Khosla, A. Review - Organic-Inorganic Hybrid Functional Materials: An Integrated Platform for Applied Technologies. *J. Electrochem. Soc.* **2018**, *165*, B3137−B3156.

(4) Faustini, M.; Nicole, L.; Ruiz-Hitzky, E.; Sanchez, C. History of Organic−Inorganic Hybrid Materials: Prehistory, Art, Science, and Advanced Applications. *Adv. Funct. Mater.* **2018**, *28*, 1704158.

(5) Sanchez, C.; Boissiere, C.; Cassaignon, S.; Chaneac, C.; Durupthy, O.; Faustini, M.; Grosso, D.; Laberty-Robert, C.; Nicole, L.; Portehault, D.; Ribotm, F.; Rozes, L.; Sassoye, C. Molecular Engineering of Functional Inorganic and Hybrid Materials. *Chem. Mater.* **2014**, *26*, 221−238.

(6) Lebeau, B.; Innocenzi, P. Hybrid Materials for Optics and Photonics. *Chem. Soc. Rev.* **2011**, *40*, 886−906.

(7) Coronado, E.; Galán-Mascarós, J. R.; Gómez-García, C. J.; Laukhin, V. Coexistence of Ferromagnetism and Metallic Conductivity in a Molecule-Based Layered Compound. *Nature* **2000**, *408*, 447−449.

(8) Yang, S.; Niu, W.; Wang, A. L.; Fan, Z.; Chen, B.; Tan, C.; Lu, Q.; Zhang, H. Ultrathin Two-Dimensional Organic−Inorganic Hybrid Perovskite Nanosheets with Bright, Tunable Photoluminescence and High Stability. *Angew. Chem., Int. Ed.* **2017**, *56*, 4252−4255.

(9) Brenner, T. M.; Egger, D. A.; Kronik, L.; Hodes, G.; Cahen, D. Hybrid Organic - Inorganic Perovskites: Low-Cost Semiconductors with Intriguing Charge-Transport Properties. *Nat. Rev. Mater.* **2016**, *1*, 15007.

(10) Liu, J.; Yoon, B.; Kuhlmann, E.; Tian, M.; Zhu, J.; George, S. M.; Lee, Y. C.; Yang, R. Ultralow Thermal Conductivity of Atomic/Molecular Layer-Deposited Hybrid Organic-Inorganic Zincone Thin Films. *Nano Lett.* **2013**, *13*, 5594−5599.

(11) Nugent, J. L.; Moganty, S. S.; Archer, L. A. Nanoscale Organic Hybrid Electrolytes. *Adv. Mater.* **2010**, *22*, 3677−3680.

(12) Jung, J. H.; Lee, J. H.; Shinkai, S. Functionalized Magnetic Nanoparticles as Chemosensors and Adsorbents for Toxic Metal Ions in Environmental and Biological Fields. *Chem. Soc. Rev.* **2011**, *40*, 4464−4474.

(13) Kim, Y. H.; Cho, H.; Heo, J. H.; Kim, T. S.; Myoung, N. S.; Lee, C. L.; Im, S. H.; Lee, T. W. Multicolored Organic/Inorganic Hybrid Perovskite Light-Emitting Diodes. *Adv. Mater.* **2015**, *27*, 1248−1254.

(14) Wright, M.; Uddin, A. Organic-Inorganic Hybrid Solar Cells: A Comparative Review. *Sol. Energy Mater. Sol. Cells* **2012**, *107*, 87−111.

(15) Zhao, Q.; Tu, Z.; Wei, S.; Zhang, K.; Choudhury, S.; Liu, X.; Archer, L. A. Building Organic/Inorganic Hybrid Interphases for Fast Interfacial Transport in Rechargeable Metal Batteries. *Angew. Chem.* **2018**, *130*, 1004−1008.

(16) Lee, L.; Yoon, K. H.; Jung, J. W.; Yoon, H. R.; Kim, H.; Kim, S. H.; Song, S. Y.; Park, K. S.; Sung, M. M. Ultra Gas-Proof Polymer Hybrid Thin Layer. *Nano Lett.* **2018**, *18*, 5461−5466.

(17) Sharma, R. K.; Sharma, S.; Dutta, S.; Zboril, R.; Gawande, M. B. Silica-Nanosphere-Based Organic-Inorganic Hybrid Nanomaterials: Synthesis, Functionalization and Applications in Catalysis. *Green Chem.* **2015**, *17*, 3207−3230.

(18) Lee, B. H.; Min, K. R.; Choi, S. Y.; Lee, K. H.; Im, S.; Sung, M. M. Rapid Vapor-Phase Fabrication of Organic-Inorganic Hybrid Superlattices with Monolayer Precision. *J. Am. Chem. Soc.* **2007**, *129*, 16034−16041.

(19) Wang, S.; Kang, Y.; Wang, L.; Zhang, H.; Wang, Y.; Wang, Y. Chemical Organic/Inorganic Hybrid Sensors: A Review. *Sens. Actuators, B* **2013**, *182*, 467−481.

(20) Wager, J. F. Flat-Panel-Display Backplanes: LTPS or IGZO for AMLCDs or AMOLED Displays? *Inf. Display* **2014**, *30*, 26−29.

(21) Um, J. G.; Jeong, D. Y.; Jung, Y.; Moon, J. K.; Jung, Y. H.; Kim, S.; Kim, S. H.; Lee, J. S.; Jang, J. Active-Matrix GaN μ-LED Display

Using Oxide Thin-Film Transistor Backplane and Flip Chip LED Bonding. *Adv. Electron. Mater.* **2019**, *5*, 1800617.
(22) Malinowski, P. E.; Ke, T. H.; Nakamura, A.; Liu, Y. H.; Vander Velpen, D.; Vandenplas, E.; Papadopoulos, N.; Kronemeijer, A. J.; van der Steen, J. L.; Steudel, S.; Kuo, C.-C.; Huang, Y.-Y.; Chen, Y.-H.; Yeh, M.-H.; Gelinck, G.; Heremans, P. High Resolution Photolithography for Direct View Active Matrix Organic Light-Emitting Diode Augmented Reality Displays. *J. Soc. Inf. Disp.* **2018**, *26*, 128−136.
(23) Myny, K. The Development of Flexible Integrated Circuits Based on Thin-Film Transistors. *Nat. Electron.* **2018**, *1*, 30−39.
(24) Kamiya, T.; Nomura, K.; Hosono, H. Present Status of Amorphous In−Ga−Zn−O Thin-Film Transistors. *Sci. Technol. Adv. Mater.* **2010**, *11*, 044305.
(25) Street, R. A. *Hydrogenated Amorphous Silicon*; Cambridge University Press: Cambridge, U.K., 1991.
(26) Kumar, B.; Kaushik, B. K.; Negi, Y. S. Organic Thin Film Transistors: Structures, Models, Materials, Fabrication, and Applications: A Review. *Polym. Rev.* **2014**, *54*, 33−111.
(27) Ahn, C. H.; Senthil, K.; Cho, H. K.; Lee, S. Y. Artificial semiconductor/insulator superlattice channel structure for high-performance oxide thin-film transistors. *Sci. Rep.* **2013**, *3*, 2737.
(28) Chhowalla, M.; Jena, D.; Zhang, H. Two-Dimensional Semiconductors for Transistors. *Nat. Rev. Mater.* **2016**, *1*, 16052.
(29) Fortunato, E.; Barquinha, P.; Martins, R. Oxide Semiconductor Thin-Film Transistors: A Review of Recent Advances. *Adv. Mater.* **2012**, *24*, 2945−2986.
(30) Jeong, J. K. Photo-Bias Instability of Metal Oxide Thin Film Transistors for Advanced Active Matrix Displays. *J. Mater. Res.* **2013**, *28*, 2071−2084.
(31) Kim, J.; Bang, J.; Nakamura, N.; Hosono, H. Ultra-Wide Bandgap Amorphous Oxide Semiconductors for NBIS-Free Thin-Film Transistors. *APL Mater.* **2019**, *7*, 022501.
(32) Lin, Y. H.; Faber, H.; Labram, J. G.; Stratakis, E.; Sygellou, L.; Kymakis, E.; Hastas, N. A.; Li, R.; Zhao, K.; Amassian, A.; Treat, N. D.; McLachlan, M.; Anthopoulos, T. D. High Electron Mobility Thin-Film Transistors Based on Solution-Processed Semiconducting Metal Oxide Heterojunctions and Quasi-Superlattices. *Adv. Sci.* **2015**, *2*, 1500058.
(33) Chen, Y.; Huang, W.; Sangwan, V. K.; Wang, B.; Zeng, L.; Wang, G.; Huang, Y.; Lu, Z.; Bedzyk, M. J.; Hersam, M. C.; Marks, T. J.; Facchetti, A. Polymer Doping Enables a Two-Dimensional Electron Gas for High-Performance Homojunction Oxide Thin-Film Transistors. *Adv. Mater.* **2019**, *31*, 1805082.
(34) Khim, D.; Lin, Y. H.; Anthopoulos, T. D. Impact of Layer Configuration and Doping on Electron Transport and Bias Stability in Heterojunction and Superlattice Metal Oxide Transistors. *Adv. Funct. Mater.* **2019**, *29*, 1902591.
(35) Faber, H.; Das, S.; Lin, Y. H.; Pliatsikas, N.; Zhao, K.; Kehagias, T.; Dimitrakopulos, G.; Amassian, A.; Patsalas, P. A.; Anthopoulos, T. D. Heterojunction Oxide Thin-Film Transistors with Unprecedented Electron Mobility Grown from Solution. *Sci. Adv.* **2017**, *3*, No. e1602640.
(36) Lee, M.; Jo, J. W.; Kim, Y. J.; Choi, S.; Kwon, S. M.; Jeon, S. P.; Facchetti, A.; Kim, Y. H.; Park, S. K. Corrugated Heterojunction Metal-Oxide Thin-Film Transistors with High Electron Mobility via Vertical Interface Manipulation. *Adv. Mater.* **2018**, *30*, 1804120.
(37) Choi, H. H.; Rodionov, Y. I.; Paterson, A. F.; Panidi, J.; Saranin, D.; Kharlamov, N.; Didenko, S. I.; Anthopoulos, T. D.; Cho, K.; Podzorov, V. Accurate Extraction of Charge Carrier Mobility in 4-Probe Field-Effect Transistors. *Adv. Funct. Mater.* **2018**, *28*, 1707105.
(38) Chen, X.; Zhang, G.; Wan, J.; Guo, T.; Li, L.; Yang, Y.; Wu, H.; Liu, C. Transparent and Flexible Thin-Film Transistors with High Performance Prepared at Ultralow Temperatures by Atomic Layer Deposition. *Adv. Electron. Mater.* **2019**, *5*, 1800583.
(39) Yoon, M.; Park, J.; Tran, D. C.; Sung, M. M. Fermi-Level Engineering of Atomic Layer-Deposited Zinc Oxide Thin Films for a Vertically Stacked Inverter. *ACS Appl. Electron. Mater.* **2020**, *2*, 537−544.
(40) Chan, M. Y.; Komatsu, K.; Li, S. L.; Xu, Y.; Darmawan, P.; Kuramochi, H.; Nakaharai, S.; Aparecido-Ferreira, A.; Watanabe, K.; Taniguchi, T.; Tsukagoshi, K. Suppression of Thermally Activated Carrier Transport in Atomically Thin MoS2 on Crystalline Hexagonal Boron Nitride Substrates. *Nanoscale* **2013**, *5*, 9572−9576.
(41) Fishchuk, I. I.; Kadashchuk, A.; Bhoolokam, A.; De Jamblinne De Meux, A.; Pourtois, G.; Gavrilyuk, M. M.; Köhler, A.; Bässler, H.; Heremans, P.; Genoe, J. Interplay between Hopping and Band Transport in High-Mobility Disordered Semiconductors at Large Carrier Concentrations: The Case of the Amorphous Oxide InGaZnO. *Phys. Rev. B: Condens. Matter Mater. Phys.* **2016**, *93*, 195204.
(42) Zhang, P.; Wang, H.; Yan, D. Organic High Electron Mobility Transistors Realized by 2D Electron Gas. *Adv. Mater.* **2017**, *29*, 1702427.
(43) Jeong, J. Quantum-Mechanical Analysis of Amorphous Oxide-Based Thin-Film Transistors. *IEEE J. Electron Devices Soc.* **2017**, *5*, 182−187.
(44) Bukke, R. N.; Mude, N. N.; Saha, J. K.; Jang, J. High Performance of A-IZTO TFT by Purification of the Semiconductor Oxide Precursor. *Adv. Mater. Interfaces* **2019**, *6*, 1900277.
(45) Oh, H.; Park, S. H. K.; Ryu, M. K.; Hwang, C. S.; Yang, S.; Kwon, O. S. Improved Stability of Atomic Layer Deposited ZnO Thin Film Transistor by Intercycle Oxidation. *ETRI J.* **2012**, *34*, 280−283.
(46) Sheng, J.; Hong, T.; Kang, D.; Yi, Y.; Lim, J. H.; Park, J. S. Design of InZnSnO Semiconductor Alloys Synthesized by Supercycle Atomic Layer Deposition and Their Rollable Applications. *ACS Appl. Mater. Interfaces* **2019**, *11*, 12683−12692.
(47) Zhong, D. Y.; Li, J.; Zhao, C. Y.; Huang, C. X.; Zhang, J. H.; Li, X. F.; Jiang, X. Y.; Zhang, Z. L. Enhanced Electrical Performance and Negative Bias Illumination Stability of Solution-Processed InZnO Thin-Film Transistor by Boron Addition. *IEEE Trans. Electron Devices* **2018**, *65*, 520−525.
(48) Park, J.; Seth, J.; Cho, S.; Sung, M. M. Hybrid Multilayered Films Comprising Organic Monolayers and Inorganic Nanolayers for Excellent Flexible Encapsulation Films. *Appl. Surf. Sci.* **2020**, *502*, 144109.
(49) Cho, S.; Han, G.; Kim, K.; Sung, M. M. High-Performance Two-Dimensional Polydiacetylene with a Hybrid Inorganic-Organic Structure. *Angew. Chem., Int. Ed.* **2011**, *50*, 2742−2746.

https://dx.doi.org/10.1021/acs.nanolett.0c00859
Nano Lett. 2020, 20, 4864−4871